SCIENCE CHINA
Information Sciences

• RESEARCH PAPER •

March 2024, Vol. 67, Iss. 3, 132403:1–132403:10
https://doi.org/10.1007/s11432-023-3870-1

Wearable ultrasensitive and rapid human physiological monitoring based on microfiber Sagnac interferometer

Xin WANG[1], Hongyou ZHOU[1], Meihua CHEN[1], Yongcheng HE[1], Zhishen ZHANG[2*], Jiulin GAN[1*] & Zhongmin YANG[1]

[1]*State Key Laboratory Luminescent Materials and Devices, Institute of Optical Communication Materials, Special Glass Fiber and Device Engineering Technology Research and Development Center of Guangdong Province, Guangdong Provincial Key Laboratory of Fiber Laser Materials and Applied Techniques, South China University of Technology, Guangzhou* 510640*, China;*
[2]*Guangdong-Hong Kong-Macao Joint Laboratory for Intelligent Micro-Nano Optoelectronic Technology, Foshan University, Foshan* 528000*, China*

Received 21 June 2023/Revised 22 August 2023/Accepted 21 September 2023/Published online 19 February 2024

Abstract High-sensitive and fast-responding flexible strain sensors are essential for the smart wearable devices that precisely and dynamically perceive the weak deformations induced by human physiological signals. Here, a flexible strain sensor via polydimethylsiloxane (PDMS)-encapsulated microfiber Sagnac interferometer was designed and prepared for monitoring the human pulse signals and sound vibrations. The sensor achieved a record-breaking sensitivity (gauge factor, GF = 9977) and an extremely low detection limit (0.00025%) due to the strong polarization-dependent coupling effect in the microfiber coupler and the polarization-mixing effect in the Sagnac loop. The relative intensity demodulation method also enabled a fast response time of 10 μs. The wearable pulse measurements were implemented by attaching this flexible strain sensor directly to human skin at various locations and the waveform details were accurately captured. Taking advantage of the ultra-high sensitivity and fast response performance of the prepared sensor, the real-time dynamic acquisition of the underwater weak signal, such as the hydro-acoustic waves with a wide range of 20 Hz–16.86 kHz, has been demonstrated. These initial results pave the way for a new and innovative category of underwater wearable devices with rapid detection of human physiological signals and weak environmental vibrations.

Keywords flexible strain sensor, microfiber Sagnac interferometer, underwater detection

1 Introduction

Flexible strain sensors, as the intelligent skin-like devices to realize the tactile communication interface, have attracted remarkable attention for applications such as health monitoring [1, 2], human-machine interaction [3, 4], and soft robotics [5–7]. Compared to traditional rigid products, flexible strain sensors have the advantages of good flexibility and scalability, even allowing for free bending and folding. The primary aim of a flexible strain sensor is to detect the large deformations under body motion, which requires the highly elastic materials to broaden the sensing range. However, most of these sensors have limited sensitivity and response time [8], and obtusely react to the weak stimulations, such as the human physiological signals and the environmental micro-disturbances. The detection of a weak signal with a high repetition rate plays a critical role in finding the new early diagnostic marker and controlling the precision motion of the biomimetic robotic arm. Therefore, improving the sensitivity and response speed of flexible strain sensors has become an urgent issue.

To achieve high sensitivity and fast response time, several types of electronic flexible sensors have been designed, such as piezoelectric [9–11], friction [12, 13], resistive [14, 15], and capacitive [16, 17] sensors. However, the electronic sensors are fundamentally susceptible to the electroconductive liquids, and require additional waterproof structure for the applications in the underwater environments. Compared to

* Corresponding author (email: zhangzs@fosu.edu.cn, msgan@scut.edu.cn)

electronic sensors, flexible optical sensors [18, 19] intrinsically possess superior compatibility in solutions while maintaining excellent sensing performance. Over the past decades, optical fiber sensors [20, 21] have been extensively used on complex curved surfaces to measure strain with high accuracy and high speed. To further improve the sensitivity and flexibility, the encapsulation of optical micro/nanofibers in flexible films has been the most competitive candidate for the flexible strain sensors with micro strain measurement, lower power consumption, and compact structures [22].

Micro/nanofiber flexible sensors are designed according to two main stress response parameters: the optical loss and the optical path. For the sensors based on the optical loss principle, the force induced by the environmental disturbance on the sensor will change the radius of the microfiber, increase the leakage energy of the guiding mode in the flexible film, and further increase the scattering loss. For example, Zhang et al. [23] demonstrated a flexible microfiber pressure sensor with a detection limit of 7 mPa. An airflow sensor based on a U-shaped microfiber sensor encapsulated in a polydimethylsiloxane (PDMS) film realized a resolution of 0.012 $\mathrm{m{\cdot}s^{-1}}$ [24]. Zhu et al. [25] designed a stretchable and ultra-thin optical sensor based on a self-assembled wavy microfiber and achieved a detection limit of 0.5%. Pan et al. [26] further reduced the detection limit to 0.25% based on a pre-bent microfiber sensor. However, a more sensitive sensor of the depletion type is inevitably operated over a higher loss region, which makes the sensing signal easily submerged in the noise. Compared with the depletion type sensor, the optical path type sensor has a smaller insertion loss and a higher signal noise ratio. The flexible microfiber strain sensors based on the optical path principle can achieve a higher sensitivity because the tiny optical path difference is converted to a significant change in intensity and wavelength shift by the interference effect. The detection limit of the interferometric sensor was simply reduced by increasing the power. Li et al. [27] proposed a hybrid plasmonic microfiber knot resonator for weak strain measurement with a detection limit of 0.01%. Yu et al. [28] designed a strain sensor based on two evanescently coupled micro/nanofibers encapsulated in a flexible PDMS film with a strain resolution of 0.0012%. Wang et al. [29] proposed a flexible optical fiber strain sensor with an ultra-low detection limit of 0.001% based on a microfiber coupler encapsulated in a PDMS film. To further reduce the detection limit of the sensor, the innovative exploration in optical interferometer structure is required. The optical fiber Saganc interferometer, consisting of a fiber coupler and a silica loop region, offers higher resistance to unintentional environmental influences due to the reciprocal structure.

Here, we proposed a novel high-sensitive and fast-responding strain flexible sensor based on the Sagnac interferometer with the microfiber coupler encapsulated in PDMS films. The microstrain induced change in coupling length will lead to a drastic change in the coupling radio due to the strong coupling effect in the microfiber Sagnac interferometer. The sensor demonstrated a gauge factor (GF) up to 9977 in the strain range of 0%–0.008%, a high strain resolution of 0.00025% which corresponds to 100 nm elongation on a 4-cm length device, and a fast temporal frequency response up to 50 kHz for sound detection. These excellent abilities have enabled the microfiber Sagnac interferometer sensor to operate in underwater environments. As a proof-of-concept, the human pulse waves and the weak environmental vibrations (20 Hz–16.86 kHz) are accurately measured underwater. The proposed flexible microfiber Sagnac interferometer sensor with high sensitivity and fast response speed exhibits great potential for monitoring ultra-weak physiological signals and high-frequency weak vibrations in the solution environments.

2 Flexible strain sensing system

The mechanism diagram of the flexible strain sensing system based on the microfiber Sagnac interferometer is shown in Figure 1. To make a Sagnac interferometer, a single-mode fiber was bent to a loop and the two free ends were twisted together. The twisted region was laterally fused and tapered to a microfiber coupler by using the flame-brushing method [30]. To reduce the insertion loss, a hydroxide flame and a computer-controlled high-precision translation stage (ESP301, Newport) were used to control the required diameter of the microfiber. The power transmission of the microfiber Sagnac interferometer was monitored in real-time during the fabrication procedure. Once the fiber had been heated to a softening temperature, it was pulled in the horizontal plane until the detection power had reached the designed coupling ratio. The typical measured loss of the prepared microfiber coupler was about 0.1 dB.

The prepared microfiber coupler of the Sagnac interferometer was further packaged in the flexible films to improve its flexibility and to ensure long-term stability in the water environment. PDMS, a highly flexible, biocompatible and hydrophilic polymer, was chosen as the encapsulation material. It was

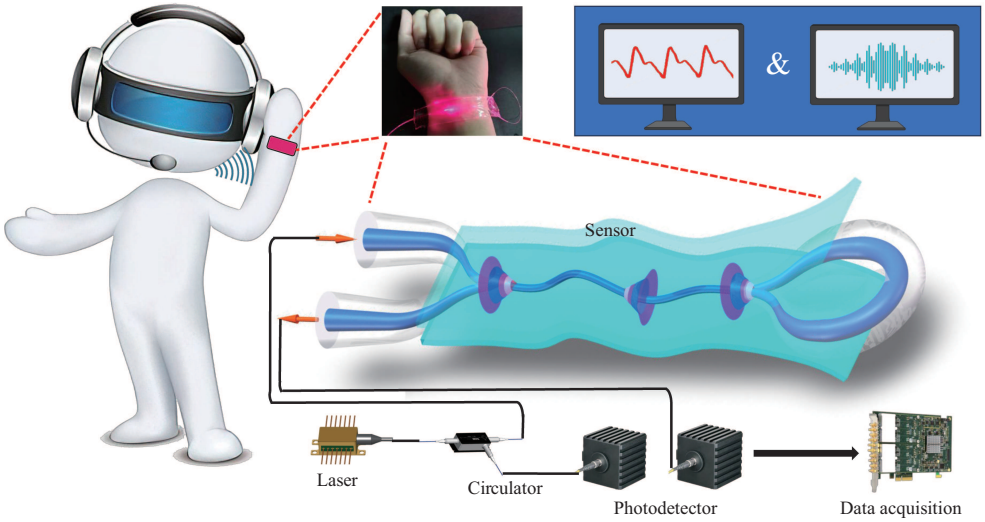

Figure 1 (Color online) Mechanism diagram of flexible microfiber Sagnac interferometer sensors.

worth emphasizing that the PDMS coating not only prevented the microfiber from external dust but also strengthened the evanescent fields outside the microfiber due to a lower refractive index (RI) contrast, which made the microfiber sensor more susceptible to micro-strain. Degassed PDMS (base : curing agent = 10 : 1) was applied to a glass substrate to form a consistent layer and then heated at 80°C for 20 min to cure. Then, the fabricated microfiber coupler was transferred to the PDMS film, where it would stick by van der Waals and electrostatic forces. Some residual PDMS was poured onto the microfiber coupler and the PDMS-microfiber coupler-PDMS sandwich structure was realized. After packaging, the insertion loss of the encapsulated microfiber coupler was up to 1.5 dB. The PDMS-encapsulated microfiber sensor was more transferable than the bared microfiber. The PDMS-encapsulated microfiber sensor was non-destructively separated from the attached platform by using the interface lubricative effect of alcohol solvent, and was attached to human skin by using the wettability of alcohol surfactant, which easily volatilizes and does not react with PDMS film. The inset showed the prepared PDMS-encapsulated microfiber Sagnac interferometer sensor, which was attached tightly to the wrist and indicated the good wearability. The evanescent light field in the PDMS was also clearly observed to ensure a high sensitivity.

For the experimental strain measurements, a 1550 nm, 1.1 MHz linewidth distributed feedback (DFB) laser diode (FITEL, Furukawa Electric Co.) and two photodetectors (Thorlabs PDA50B-EC) were used as the light source and detectors, respectively. The PDMS film embedded microfiber Sagnac interferometer sensor was attached and clamped on a translation stage and the applied strain could be accurately controlled. The strain was defined as the change in length relative to the original, e.g., 10 μm strain on a 1 cm initial PDMS film was equivalent to 0.1% strain. It is noteworthy that the strain should increase gradually to avoid the fracture of the microfiber sensor during the test.

3 Results and discussion

3.1 Optical and mechanical properties of PDMS films

For realizing a high-performance flexible strain sensor, the optical and mechanical properties of the PDMS films should be well matched to the microfiber. As the encapsulation material, the PDMS films were the cladding layer for guiding the evanescent fields of the microfiber mode and required good light conductivity and a lower RI than the microfiber ($n_1 = 1.444$). As shown in Figure 2(a), the 500 μm thickness PDMS samples with the base material to curing agent mixing ratio of 5 : 1, 10 : 1, and 20 : 1 all possessed good transmittance (>90%) in the 300–800 nm wavelength range. The RI of PDMS with a mixing ratio of 5 : 1, 10 : 1, and 20 : 1 mixing ratios were measured to be 1.4023, 1.4019, and 1.3996 at a wavelength of 1533 nm (Figure 2(b)). Due to the preferred optical characteristics of PDMS, the additional loss of the microfiber Sagnac interferometer after the packaging process was approximately 3 dB. As a strain sensing material, the PDMS films also required high elasticity and the recoverable property to enhance the strain sensitivity and stability of the sensor. Figure 2(c) showed that the PDMS with 10 : 1 mixing ratio had

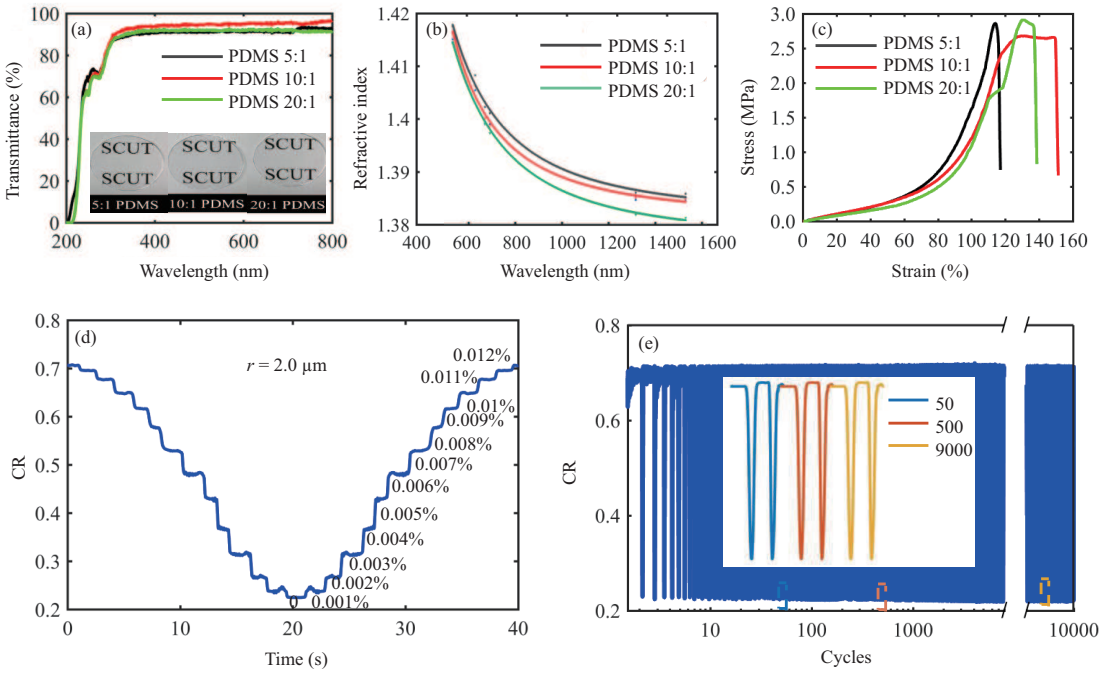

Figure 2 (Color online) (a) Transmittance of PDMS diaphragms at different wavelengths with different proportions; (b) refractive index of PDMS diaphragms at different wavelengths with different proportions; (c) stress-strain curves of PDMS diaphragms with different proportions; (d) a cycling test when the strain was changed between 0% and 0.012% at intervals of 0.001%; (e) time-dependent strain-CR response produced by an optical microfiber Sagnac interferometer sensor during the periodic stretch and release with 0.012% strain over 10000 cycles.

a maximum fracture strain of 149.43%, which was set as the best ratio for the packaging composites. Figure 2(d) shows the time-dependent strain-CR response (CR $= P_2/((P_2 + P_1'))$, where P_2 and P_1' are the intensities of output port 2 and output port 1 of the strain sensor) of the sensor in a stretch and release cycle, with each step corresponding to $0.001\%\varepsilon$. The symmetrical response curve indicated good reversibility of the sensor. The sensor was automatically stretched and released 10000 times with an elongation ranging from 0% to 0.012% and the CR curves remained stable and reversible throughout all cycles, as shown in Figure 2(e). The response curves of the 50-th, 500-th, and 9000-th tests were almost identical in the inset of Figure 2(e), a clear indication of excellent stability and repeatability.

3.2 Principle and sensing performances of flexible microfiber Sagnac interferometer

To investigate the relationship between CR and strain in detail, the basic principle of the microfiber Sagnac interferometer sensor was theoretically analyzed. Due to the elliptical cross section of the coupling microfibers, the strong birefringence effect was considered, and $C_{x/y}$ were the coupling coefficients of x/y-polarizations [31]. The input laser with power P_1 was set as naturally polarized light with 50% horizontal polarization component and 50% vertical polarization component.

$$\boldsymbol{E}_{1\text{in}} = \begin{bmatrix} E_{1x} \\ E_{1y} \end{bmatrix} = \begin{bmatrix} \sqrt{P_1/2} \\ \sqrt{P_1/2} \end{bmatrix}. \tag{1}$$

When the 1550 nm laser was injected into port 1, the input light was split into two beams (ports 3 and 4) after the coupling region. The Sagnac loop was set as a polarization rotator with a rotation angle θ. Thus, the light in port 3 would rotate its polarization angle θ and then pass through the coupling region a second time. Conversely, the light in port 4 would rotate its polarization angle $-\theta$, pass through the coupling region and finally cause the optical interference in both output ports 1 and 2 [32]. The specific theoretical analysis is as follows. After the second coupling effect, the first part of light in port 2 was calculated as

$$\boldsymbol{E}_{2\text{out}} = \begin{bmatrix} \sin(C_x L) & 0 \\ 0 & \sin(C_y L) \end{bmatrix} \cdot \boldsymbol{R} \cdot \begin{bmatrix} \sin(C_x L) & 0 \\ 0 & \sin(C_y L) \end{bmatrix} \cdot \boldsymbol{E}_{1\text{in}}, \tag{2}$$

where L was the coupling length. $\boldsymbol{R}$ was rotation matrix of the polarization state.

$$\boldsymbol{R} = \begin{bmatrix} \cos\theta & -\sin\theta \\ \sin\theta & \cos\theta \end{bmatrix}. \tag{3}$$

Similarly, the second part of light in port 2 was calculated as

$$\boldsymbol{E}'_{2\text{out}} = \begin{bmatrix} \mathrm{j}\cdot\cos(C_x L) & 0 \\ 0 & \mathrm{j}\cdot\cos(C_y L) \end{bmatrix} \cdot \boldsymbol{R}^{-1} \cdot \begin{bmatrix} \mathrm{j}\cdot\cos(C_x L) & 0 \\ 0 & \mathrm{j}\cdot\cos(C_y L) \end{bmatrix} \cdot \boldsymbol{E}_{1\text{in}}. \tag{4}$$

The total output electric field in port 2 was

$$\boldsymbol{E}_2 = \boldsymbol{E}_{2\text{out}} + \boldsymbol{E}'_{2\text{out}}. \tag{5}$$

The coupling radio was defined as the radio between the total output power in port 2 and the total input power in port 1.

$$\mathrm{CR} = \frac{P_2}{P_1} = \frac{(\boldsymbol{E}_2^*)^{\mathrm{T}} \cdot \boldsymbol{E}_2}{P_1}. \tag{6}$$

By submitting (1)–(5) into (6), the CR was simplified as

$$\mathrm{CR} = \frac{1}{2}\{\cos(2C_x L)\cos\theta + \cos[(C_x - C_y)L]\sin\theta\}^2 + \frac{1}{2}\{\cos(2C_y L)\cos\theta - \cos[(C_x - C_y)L]\sin\theta\}^2. \tag{7}$$

Based on (7), the CR was the combination of the fast oscillating items $\cos(2C_x L)$ and $\cos(2C_y L)$, and the slow oscillating item $\cos[(C_x - C_y)L]$, where $2C_x \gg (C_x - C_y)$ and $2C_y \gg (C_x - C_y)$. When θ tends 0, the weight coefficient $(\sin\theta)$ of the slow oscillating item tends 0, which means that the CR had a shorter cycle length and was more sensitive to the coupling length L. To discuss the highly sensitive situations, θ was set to 0 in the following theoretical analysis. The CR expression could be approximated as follows:

$$\mathrm{CR} = \frac{1}{2}\{\cos(2C_x L)\}^2 + \frac{1}{2}\{\cos(2C_y L)\}^2. \tag{8}$$

When the external strain ε was applied in the coupling region, the coupling length L, the RI of microfiber, and the RI of the PDMS were changed. The length variation was

$$\Delta L = \varepsilon L. \tag{9}$$

The change in RI was expressed as

$$\Delta n = -n^3\varepsilon[p_{12} - \nu(p_{11} + p_{12})], \tag{10}$$

where ν, p_{11}, and p_{12} were the Poisson's ratio and elastic coefficients, respectively [33,34]. The Δn would directly lead to the change in the coupling coefficients ΔC_x and ΔC_y. As shown in Figure 3(a), the CR curve shifted to the right with increasing strain ε.

When ε was small enough, the change in CR was given by the following equation:

$$\Delta\mathrm{CR} = \frac{\partial\mathrm{CR}}{\partial C_x}\cdot\Delta C_x + \frac{\partial\mathrm{CR}}{\partial C_y}\cdot\Delta C_y + \frac{\partial\mathrm{CR}}{\partial L}\cdot\Delta L. \tag{11}$$

Based on (11), the applied strain could be obtained by demodulating the ΔCR. The strain sensitivity was evaluated by the GF:

$$\mathrm{GF} = \left|\frac{\Delta\mathrm{CR}}{\varepsilon}\right| = L\cdot\left|\sin(4C_x L)\cdot\left(2C_x + \frac{\Delta C_x}{\varepsilon}\right) + \sin(4C_y L)\cdot\left(2C_y + \frac{\Delta C_y}{\varepsilon}\right)\right|. \tag{12}$$

According to (12), the GF could achieve a larger value with increasing L, C_x and C_y. Since C_x and C_y increased with decreasing microfiber radius r, the microfiber Sagnac interferometer sensor was more sensitive with a thinner microfiber and a longer coupling length. As shown in Figure 3(b), the optimum theoretical value of the GF could reach 23000 with $r = 0.5$ μm.

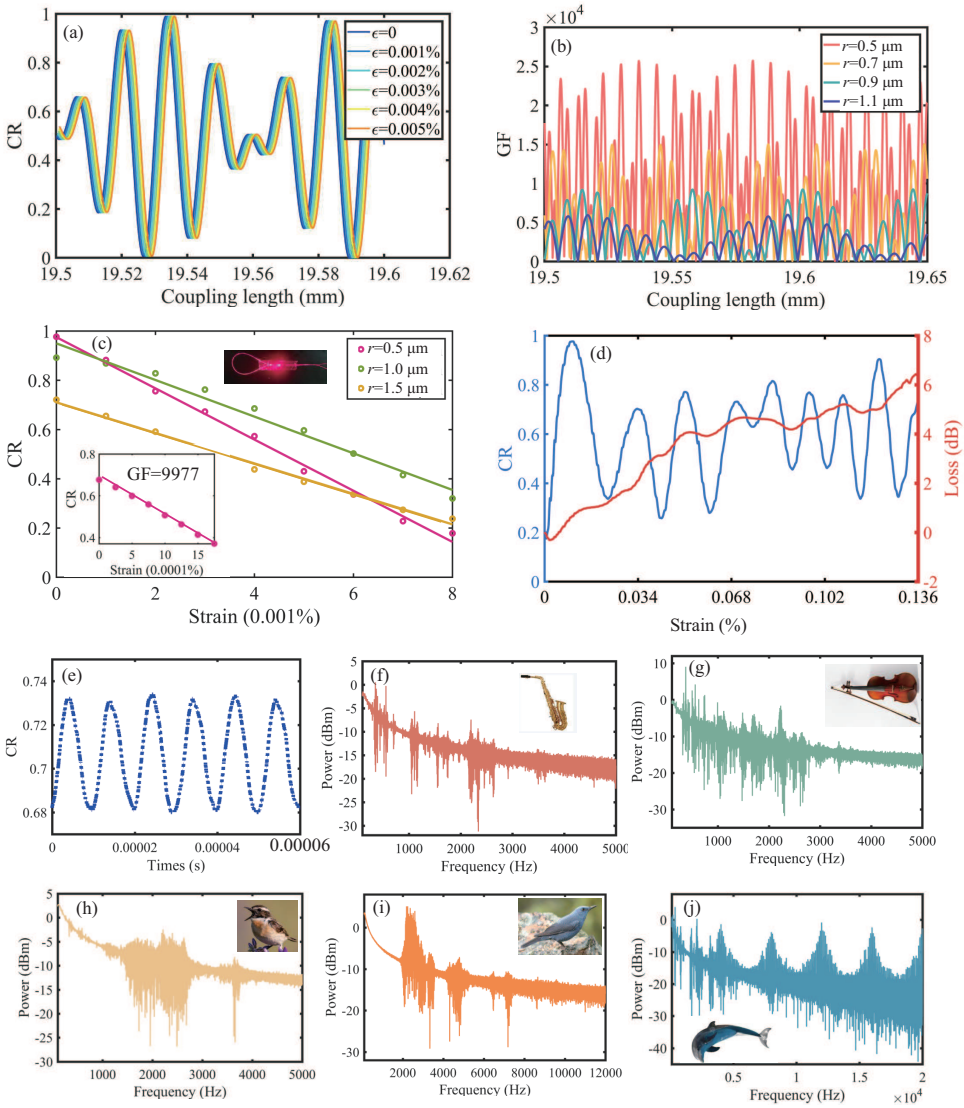

Figure 3 (Color online) (a) A simulation diagram of the strain-CR response at various coupling lengths. (b) Sensitivity simulation for various coupling lengths and radii. (c) Experiment results for the strain-CR response of a microfiber Sagnac interferometer sensor with radii of 0.5, 1.0, and 1.5 μm, respectively. The inset is the related strain-CR response of a microfiber Sagnac interferometer with radii of 0.5 μm. (d) CR periodic change and loss variation of the microfiber Sagnac interferometer sensor under strain. (e) Time-dependent strain-CR response produced by a signal generator connected to a shaker to generate a frequency of 50 kHz. The frequency spectrum of the recorded CR change induced by (f) sax and (g) violin. The frequency spectrum of the recorded CR change induced by the sounds of (h) lark and (i) painted bird. (j) The frequency spectrum of the recorded CR change induced by the dolphin sound music sung by Vitas.

The sensing performance of our fabricated flexible microfiber Sagnac interferometer sensor was experimentally investigated using a tensile strain tester. As shown in Figure 3(c), the CR at various radii (0.5, 1.0, and 1.5 μm) exhibited a considerable degree of change trend with strain variation. The 0.5 μm-radius microfiber Sagnac interferometer sensor had the higher sensitivity, which was consistent with theoretical analysis. We also observed clear step signals in the strain-CR curve with a step of 0.00025% in the inset of Figure 3(c). These results showed that the flexible strain sensor had an extremely low detection limit and resolution (0.00025%). From the experimental data, the maximum GF of the sensor was 9977 in the strain range of 0%–0.008%. Such sensitivity was about one order of magnitude higher than the most of reported flexible strain sensors, which could be further improved by reducing the thickness of the PDMS diaphragm and the microfiber radius of the Sagnac interferometer sensor.

Due to the oscillation characteristic of the strain-CR curve, the strain sensing range within a monotonically increasing or decreasing interval would be limited to only about 0.008% for the sensor with 0.5-μm radius microfiber. To widen the sensing range while maintaining a relatively low detection limit,

the method of two-parameter CR and optical loss demodulation was adopted. The optical loss α (dB) was defined as $-10\log[(P_2+P_1')/P_1]$, where P_1 was the input light intensity. As shown in Figure 3(d), the optical loss (red curve) was monotonic with increasing strain until the strain reached 0.136%. The optical loss had a nonlinear increase curve due to the hysteresis effect of PDMS material, which limited its acting as a single sensing feature with a wide sensing range. By combining the strain-CR response and the optical loss simultaneously, the value zone of the strain could be identified by the monotonically increasing loss, and then the strain value was accurately determined by the oscillating strain-CR curve with high sensitivity. Here, the strain sensing range had been expanded to 0%–0.136% with a maximum GF of 9977. It was also worth emphasizing that the loss based dual-parameter demodulation scheme could be further extended to other sensors to achieve a wide sensing range with a low detection limit, as no additional component was required.

To investigate the response time of the fabricated sensor, the PDMS-encapsulated microfiber Sagnac interferometer was mounted on the surface of a vibration plate (ceramic chip, 25 mm diameter and 0.18 mm thickness), which was connected to the signal generator for producing the mechanical vibrations. The sensor synchronously generated a time-varying CR waveform when the mechanical load was applied. As shown in Figure 3(e), the simple harmonic vibration was clearly measured with the distinguishable details. The maximum sinusoidal frequency $f_{\max}$ was up to 50 kHz. Estimated from the Nyquist-Shannon sampling theorem $\Delta t < \frac{1}{2f_{\max}}$ [35], the response time was calculated as 10 μs.

With high sensitivity and fast response, this flexible microfiber Sagnac interferometer sensor was used to further explore the dynamic weak strain sensing ability. The sensor was suspended on a loudspeaker at a distance of 10 cm. When the sound propagated to the sensor, the thin PDMS film was repeatedly stretched and relaxed, and its deformation was instantly captured by the microfiber Sagnac interferometer to produce a synchronous oscillating CR curve. The complex frequency sounds, such as the sound of sax and violin, were chosen as the vibration source. By using the fast Fourier transform, the frequency spectrum of recorded sound was obtained. As shown in Figures 3(f) and (g), the recorded sound was mainly concentrated in the 100 Hz–3.5 kHz range. Other high frequency sounds, such as the frequency spectrum of the lark's voice (1–4 kHz) and the painted bird's voice (2–8 kHz), were clearly recorded by our sensor in Figures 3(h) and (i). To investigate the response of the flexible microfiber Sagnac interferometer sensor to the sound covering the human hearing range (20 Hz–20 kHz), dolphin sound music sung by Vitas was selected for testing. The demodulated CR change frequency spectrum under the music source clearly illustrated the details of frequency variation (Figure 3(j)), covering low, mid, and high frequency signals, demonstrating the response of the sensor to different complex frequency sound signals. The demodulated CR changes the spectrum under the music audio source, which could even reach the highest hearing limit of the human ear, 20 kHz. The above results meant that our sensor can respond to the weak high-frequency signals with high detection accuracy.

3.3 Submerged wearable sensor for detecting high frequency micro-vibrations

To illustrate the feasibility of wearable applications, respiration and arterial pulse were measured in the air. Our flexible sensor was incorporated into a medical mask to monitor the volunteer's breathing. The CR of the sensor changed regularly as the volunteer inhaled and exhaled. The rate and magnitude of respiration in the heavy, normal, and slight breathing patterns were clearly recognizable from the CR curve (Figure 4(a)). Benefiting from the good flexibility and biocompatibility of PDMS, the sensor could be attached to the surface of human skin for the arterial pulse measurement. Figure 4(b) showed the sensor attached to the wrist and fingertip of a volunteer's body (female, 25 years old), used for real-time detection of pulse signals. The sensor displayed stable and repeatable pulse waveforms with frequencies of 88 and 81 beats/min for the wrist and finger, within the normal pulse rate range (60–100 beats/min for adults). The typical characteristic peaks associated with the shock wave, the reflection waveform for the late systolic wave, and the diastolic wave could be clearly distinguished from the measured pulse waveform [36]. These results indicated that our sensor was promising for wearable health monitoring.

Taking advantage of the distinctive elastic, hydrophilic, and high-sensitive characteristics of the PDMS-encapsulated microfiber Sagnac interferometer, we have developed a novel submerged wearable sensor for monitoring weak physiological signals and detecting high frequency micro-vibrations. Compared to air, the water resistance was much greater, which significantly reduced the magnitude of deformation and required an ultra-sensitive strain sensor. As shown in Figure 4(b), our sensor was subsequently attached to the wrist and fingertip sites underwater. The repeatable pulse waveforms were obtained with the

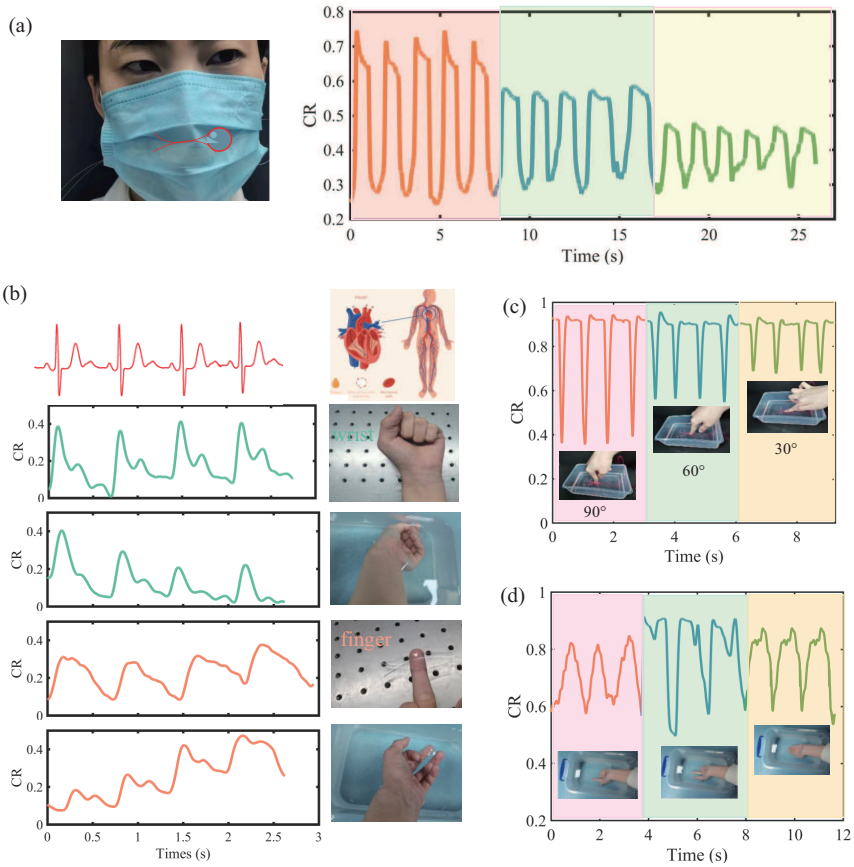

Figure 4 (Color online) (a) Monitoring the strain change of inhalation and exhalation over time using the as-fabricated optical sensor; (b) diagram of the cardiac blood circulation system and monitoring a volunteer's pulse signals at finger and wrist in air and in water; (c) monitoring different angles of fingertip bending under water; (d) observing the weak wrist movement, which was caused by the far end fingers bending.

precise vibration period by distinguishing the reflection waveform for the late systolic wave. The sloping baseline of the pulse signal was caused by the irregular vibrations of the water wave in a finite fluid container. For the underwater human-machine interaction applications, our sensor demonstrated two different types of the submerged gesture recognition. The first type was to fix the sensor on the other object in the water and then discriminate the pressure angle of the fingertip, as shown in Figure 4(c). When the fingertip was in a vertical position (90°), a strong force was exerted on the flexible microfiber Sagnac interferometer sensor, resulting in obvious changes in the CR curve. When the pressure angle between the fingertip and the horizontal line was gradually reduced to 60° and 30°, the force exerted by the fingertip gradually decreased, and the amplitude of the CR change also gradually decreased. The second type was to attach the sensor to the human body, and then discriminate the body movement under water. In Figure 4(d), the sensor on the wrist could clearly identify between different states of finger flexion and extension. The sensor had significantly different response curves by bending of different fingers and the same contour signals by repeatedly bending the same fingers. The tiny distinctions in the repeated curves were caused by the reflected water wave motion, which can be alleviated by a larger container.

To explore the sensor's capability for detecting the high frequency micro-vibrations underwater (Figure 5(a)), a flexible sensor packaging vibration plate was submerged in water. As shown in Figure 5(b), the underwater simple harmonic vibration was measured with a maximum frequency of 16.86 kHz, which was lower than the maximum vibration frequency in the air but very close to the human hearing range. Due to the effect of the surrounding water pressure, the amplitude of the higher frequency vibration (>16.86 kHz) was strongly inhibited, and the deformation of the flexible sensor was too small to measure. To listen to the sound oscillations in the water, two fiber ends of our flexible sensor were also attached to a recessed Plexiglas model holder (80 mm × 12 mm × 8 mm) with UV-curable adhesive, and the sensor was placed 10 cm under water. A loudspeaker was used to play dolphin sound music sung by

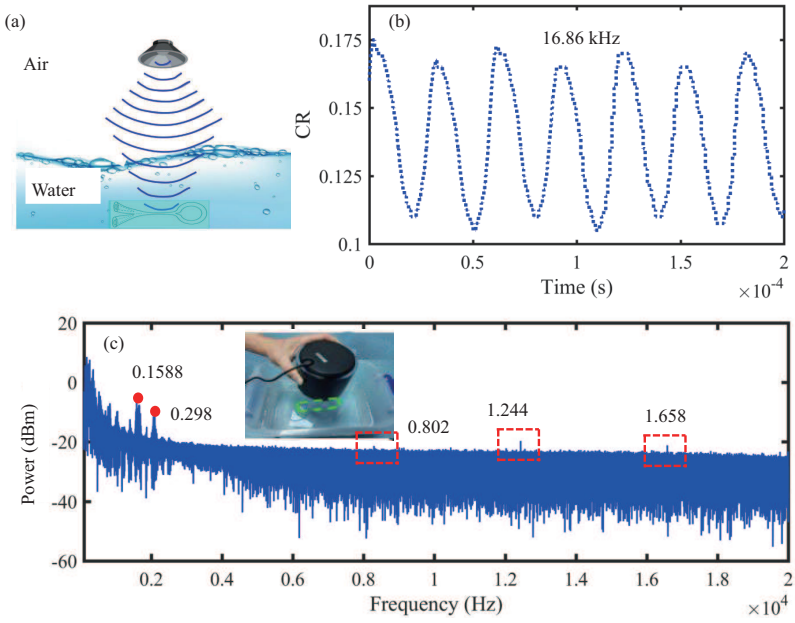

Figure 5 (Color online) (a) Schematic diagram of sound propagation under water; (b) time-dependent strain-CR response produced by ultrasonic vibrations to generate a frequency of 16.86 kHz; (c) frequency spectrum of the recorded CR change induced by the dolphin sound music sung by Vitas under water.

Vitas above the water. As the water waves attenuated the high frequency signals, the majority of the signals detected by the flexible microfiber Sagnac interferometer sensor were below 3 kHz (Figure 5(c)), and the characteristic peaks of dolphin sound at 12.44 and 16.58 kHz were still measured with 2 dB signal-to-noise ratio. Based on the characteristics of the sensor for underwater high frequency sound detection, the flexible microfiber Sagnac interferometer sensor could potentially be used as a hydrophone [11].

4 Conclusion

In summary, we have developed a highly sensitive and fast response microfiber Sagnac interferometer sensor based on the strong secondary coupling effect that is encapsulated in PDMS film. Based on the CR demodulation scheme which can eliminate interference from the external environment, this microfiber Sagnac interferometer sensor has achieved ultra-high sensitivity (GF = 9977), ultra-fast response time (10 μs), and ultra-low detection limit (0.00025%). These outstanding properties make it possible to detect weak signals such as pulse and sound vibrations in real time. Furthermore, ultra-weak signals such as pulse waves from the human body and sound vibrations with a wide range of 20 Hz–16.86 kHz have been demonstrated underwater. These initial results could pave the way for the future development of ultra-sensitive wearable optical devices and multi-functional photonic health monitoring systems. This microfiber Sagnac interferometer sensor also has the broad prospects and huge potential in future integrated applications due to its simple demodulation system, easily integrative multi-layer structure, and expandable sensing applications.

Acknowledgements This work was partially supported by National Natural Science Foundation of China (Grant No. 62075064), Local Innovative and Research Teams Project of Guangdong Pearl River Talents Program (Grant No. 2017BT01X137), Key R&D Program of Guangzhou (Grant No. 202007020003), Guangdong Basic and Applied Basic Research Foundation (Grant Nos. 2021B1515020095, 2021A1515110919), Fundamental Research Funds for the Central Universities (Grant No. 2022ZYGXZR003), and Research Fund of Guangdong-Hong Kong-Macao Joint Laboratory for Intelligent Micro-Nano Optoelectronic Technology (Grant No. 2020B1212030010).

References

1 Takei K, Honda W, Harada S, et al. Toward flexible and wearable human-interactive health-monitoring devices. Adv Healthcare Mater, 2014, 4: 487–500
2 Liu Y, Pharr M, Salvatore G A. Lab-on-skin: a review of flexible and stretchable electronics for wearable health monitoring. ACS Nano, 2017, 11: 9614–9635
3 Chao M Y, Di P J, Yuan Y, et al. Flexible breathable photothermal-therapy epidermic sensor with MXene for ultrasensitive wearable human-machine interaction. Nano Energy, 2023, 108: 108201

4 Lu L J, Jiang C P, Hu G S, et al. Flexible noncontact sensing for human-machine interaction. Adv Mater, 2021, 33: 2100218
5 Majidi C. Soft robotics: a perspective-current trends and prospects for the future. Soft Robot, 2014, 1: 5–11
6 Kim S, Laschi C, Trimmer B. Soft robotics: a bioinspired evolution in robotics. Trends Biotechnol, 2013, 31: 287–294
7 Wu H, Gao W, Yin Z P. Materials, devices and systems of soft bioelectronics for precision therapy. Adv Healthcare Mater, 2017, 6: 1700017
8 Liang H H, He Y C, Chen M H, et al. Self-powered stretchable mechanoluminescent optical fiber strain sensor. Adv Intell Syst, 2021, 3: 2100035
9 Xu H H, Lv Y, Qiu D X, et al. An ultra-stretchable, highly sensitive and biocompatible capacitive strain sensor from an ionic nanocomposite for on-skin monitoring. Nanoscale, 2019, 11: 1570–1578
10 Mannsfeld S C B, Tee B C K, Stoltenberg R M, et al. Highly sensitive flexible pressure sensors with microstructured rubber dielectric layers. Nat Mater, 2010, 9: 859–864
11 Wang J B, Yan Z L, Chen B, et al. An on-line calibration hydrophone with electrostatic actuator. Sci China Inf Sci, 2016, 59: 062311
12 He J, Fan X M, Zhao D Y, et al. A high-efficient triboelectric-electromagnetic hybrid nanogenerator for vibration energy harvesting and wireless monitoring. Sci China Inf Sci, 2022, 65: 142401
13 Kim K H, Jang N S, Ha S H, et al. Highly sensitive and stretchable resistive strain sensors based on microstructured metal nanowire/elastomer composite films. Small, 2018, 14: 1704232
14 Zhao G R, Zhang X D, Cui X, et al. Piezoelectric polyacrylonitrile nanofiber film-based dual-function self-powered flexible sensor. ACS Appl Mater Interfaces, 2018, 10: 15855–15863
15 Zhu M L, Shi Q F, He T Y, et al. Self-powered and self-functional cotton sock using piezoelectric and triboelectric hybrid mechanism for healthcare and sports monitoring. ACS Nano, 2019, 13: 1940–1952
16 Ha M, Lim S, Cho S, et al. Skin-inspired hierarchical polymer architectures with gradient stiffness for spacer-free, ultrathin, and highly sensitive triboelectric sensors. ACS Nano, 2018, 12: 3964–3974
17 Wu F, Li C J, Yin Y Y, et al. A flexible, lightweight, and wearable triboelectric nanogenerator for energy harvesting and self-powered sensing. Adv Mater Technol, 2019, 4: 1800216
18 Cai S S, Liu F, Wang R L, et al. Narrow bandwidth fiber-optic spectral combs for renewable hydrogen detection. Sci China Inf Sci, 2020, 63: 222401
19 Wang R L, Zhang H Z, Liu Q Y, et al. Operando monitoring of ion activities in aqueous batteries with plasmonic fiber-optic sensors. Nat Commun, 2022, 13: 547
20 Pan J, Jiang C P, Zhang Z, et al. Flexible liquid-filled fiber adapter enabled wearable optical sensors. Adv Mater Technol, 2020, 5:
21 Guo J, Zhou B, Zong R, et al. Stretchable and highly sensitive optical strain sensors for human-activity monitoring and healthcare. ACS Appl Mater Interfaces, 2019, 11: 33589–33598
22 Tong L, Lou J, Mazur E. Single-mode guiding properties of subwavelength-diameter silica and silicon wire waveguides. Opt Express, 2004, 12: 1025–1035
23 Zhang L, Pan J, Zhang Z, et al. Ultrasensitive skin-like wearable optical sensors based on glass micro/nanofibers. Opto-Electron Adv, 2020, 3: 19002201
24 Zhang Z, Kang Y, Yao N, et al. A multifunctional airflow sensor enabled by optical micro/nanofiber. Adv Fiber Mater, 2021, 3: 359–367
25 Zhu H T, Zhan L W, Dai Q, et al. Self-assembled wavy optical microfiber for stretchable wearable sensor. Adv Opt Mater, 2021, 9: 2002206
26 Pan J, Zhang Z, Jiang C P, et al. A multifunctional skin-like wearable optical sensor based on an optical micro-/nanofibre. Nanoscale, 2020, 12: 17538–17544
27 Li J H, Chen J H, Xu F. Sensitive and wearable optical microfiber sensor for human health monitoring. Adv Mater Technol, 2018, 3: 1800296
28 Yu W, Yao N, Pan J, et al. Highly sensitive and fast response strain sensor based on evanescently coupled micro/nanofibers. Opto-Electron Adv, 2022, 5: 210101
29 Wang X, Zhou H Y, Chen M H, et al. Highly sensitive strain sensor based on microfiber coupler for wearable photonics healthcare. Adv Intell Syst, 2022, 5: 2200344
30 Brambilla G, Finazzi V, Richardson D J. Ultra-low-loss optical fiber nanotapers. Opt Express, 2004, 12: 2258–2263
31 Payne F P, Hussey C D, Yataki M S. Polarisation analysis of strongly fused and weakly fused tapered couplers. Electron Lett, 1985, 21: 561–563
32 Liu Y E, Liu B, Feng X H, et al. High-birefringence fiber loop mirrors and their applications as sensors. Appl Opt, 2005, 44: 2382–2390
33 Dai X, Mihailov S J, Blanchetiere C. Ridge waveguide Bragg grating pressure sensor. In: Proceedings of SPIE, 2008
34 Qi K Y, Zhang Y D, Sun J F, et al. Highly sensitive strain sensor based on a sealed optical microfiber coupler. Opt Fiber Tech, 2020, 59: 102313
35 Shannon C E. Communication in the presence of noise. Proc IRE, 1949, 37: 10–21
36 Zhao K, Li Y F, Wang G X, et al. A robust QRS detection and accurate R-peak identification algorithm for wearable ECG sensors. Sci China Inf Sci, 2021, 64: 182401